AIP Advances

Demonstration of MOCVD-grown BGaN with over 10% boron composition

Cite as: AIP Advances 12, 085318 (2022); https://doi.org/10.1063/5.0113666
Submitted: 24 July 2022 • Accepted: 04 August 2022 • Published Online: 23 August 2022

Feras AlQatari, Che-Hao Liao and Xiaohang Li

Demonstration of MOCVD-grown BGaN with over 10% boron composition

Cite as: AIP Advances 12, 085318 (2022); doi: 10.1063/5.0113666
Submitted: 24 July 2022 • Accepted: 4 August 2022 •
Published Online: 23 August 2022

Feras AlQatari, Che-Hao Liao, and Xiaohang Li[a)]

AFFILIATIONS

Advanced Semiconductor Laboratory, Electrical and Computer Engineering Program, CEMSE Division, King Abdullah University of Science and Technology (KAUST), Thuwal 23955-6900, Saudi Arabia

[a)]Author to whom correspondence should be addressed: xiaohang.li@kaust.edu.sa

ABSTRACT

BGaN is an emerging ultrawide bandgap semiconductor with important applications ranging from power electronics to ultraviolet light emitters. To date, BGaN boron composition has been limited to <10% in the wurtzite phase. Herein, a 200 nm thick high quality mixed-phase BGaN film was grown via horizontal–reactor metalorganic chemical vapor deposition with boron composition exceeding 10%. The growth was performed under low temperature and pressure conditions of 600 °C and 75 Torr, respectively, with a growth rate of 0.29 μm/h. Triethylborane and triethylgallium were used as the source gases for boron and gallium, respectively. Pure nitrogen gas was used as the carrier for all reactants. A root mean square roughness value of 2.56 nm was determined using an atomic force microscopy scan on an area of 5 × 5 μm^2. X-ray diffraction (XRD) 2θ–ω scans show a nearly lattice-matched BGaN/AlN film corresponding to a boron composition of ~10%. A mixed wurtzite and zincblende phase was confirmed via an XRD pole figure and transmission electron microscopy. Additionally, the high crystalline quality of the mixed $(002)_{wz}/(111)_{ZB}$ planes was shown using an XRD rocking curve with 810 arcsec full width at half maximum. The boron composition was precisely measured as 15% using Rutherford backscattering spectrometry combined with nuclear reaction analysis.

III-nitride semiconductor materials have several technical applications in advanced optical and electronic devices.[1] III-nitrides typically crystallize in the hexagonal wurtzite phase; however, they only crystallize in the cubic zincblende phase under specific conditions because of the higher stability of the wurtzite phase of the classical nitrides AlN, GaN, and InN.[2–4] Optical devices using these wurtzite nitrides can operate over various wavelengths due to their highly tunable bandgaps from 0.7 to 6 eV.[5,6] This tunability arises from the precise selection of AlN, GaN, and InN alloys at different compositions. Metalorganic chemical vapor deposition (MOCVD) is the leading technique for the mass production of different III-nitride devices due to its flexibility in a wide selection of pressures, temperatures, chemicals, and precursor flow rates among other growth conditions. This enables MOCVD to create complex structures layering alloys under different conditions such as the common AlGaN/InGaN heterostructures in blue and ultraviolet light-emitting diodes (LEDs).

Boron-containing III-nitrides, including BAlN and BGaN, have been investigated widely due to their applications in ultraviolet and power devices.[7–18] Alloying III-nitrides with boron is useful for lattice engineering and matching within the nitride family and other materials, such as SiC and Ga_2O_3.[19,20] Additionally, alloying with boron could increase bandgaps, reduce optical absorption, and, interestingly, enable types I and II band alignments, allowing for novel device engineering.[21]

As Fig. 1 depicts, most previous studies of wurtzite BGaN, in specific, have been confined to boron compositions <3%, with the highest being 7%–7.5%.[17,22] These fall far from achieving the full range of compositions for maximum tunability of the material's properties. Many studies find a structural change from the hexagonal wurtzite phase to the cubic zincblende phase at higher boron composition films, which is confirmed in our study. Experimentally, it is typically found that as the boron incorporation increases, the film tends to have a more zincblende phase mixed with the

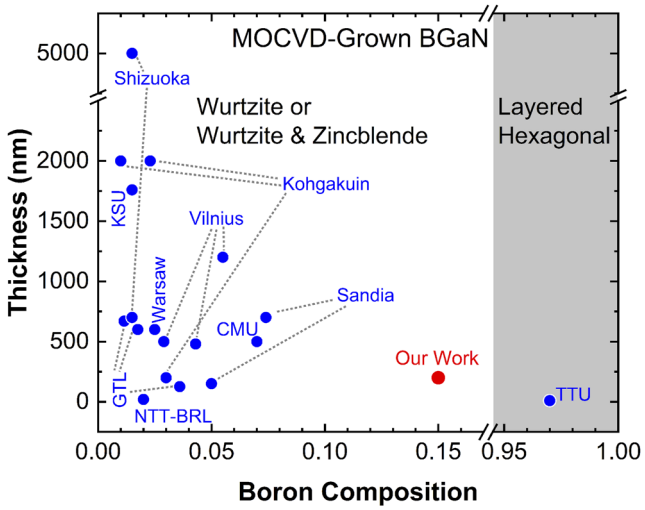

FIG. 1. Summary of notable MOCVD-grown BGaN films in literature.[8,17,18,22–24,26–37]

wurtzite.[17,23,24] Furthermore, theoretical calculations show that the cohesive energies of wurtzite and zincblende are extremely close at low compositions.[25]

Additionally, the theoretical prediction shows that the layered hexagonal phase, typically seen in pure BN, becomes more dominant at very high boron compositions.[25] This result has also been found experimentally where layered hexagonal BGaN is found at boron compositions >92%.[26]

Herein, we report the growth of a 200 nm thick, mixed-phase BGaN thin film with a boron composition of 15%. The goal of this study is to push the current limit of boron composition in BGaN films by MOCVD. The growth was performed in a Taiyo Nippon Sanso horizontal reactor MOCVD system on a commercial *c*-plane AlN(~1.3 μm)/sapphire template from Luan UV. Trimethylaluminum (TMA), triethylborane (TEB), and triethylgallium (TEG) were used as metalorganic sources. TEG is used instead of the typical trimethylgallium (TMG) for its compatibility with the low growth temperature used here.[38] Ammonia (NH_3) was used as a nitrogen source, and nitrogen gas was used as the carrier gas for the precursors. The use of nitrogen instead of hydrogen as a carrier gas has been shown to increase the crystalline quality of BGaN films by us and by others in literature (see the supplementary material).[17] The pressure and temperature were maintained at 75 Torr and 600 °C during the BGaN growth, respectively. Herein, V/III and TEB/III ratios of 2100 and 0.51 were used, respectively. The high TEB/III ratio is likely needed due to the gas phase parasitic reactions that reduce the efficiency of boron incorporation into the film.[16,22] A small growth rate and a film thickness of 0.29 μm/h and 210 nm were estimated by the reflection curves, respectively. These conditions were optimized to yield high boron compositions and crystalline quality according to the 2θ–ω peak shifts and rocking curves' (RCs) full width at half maxima (FWHM), respectively.

To characterize the surface of the BGaN film, a Bruker Dimension Icon is used to perform atomic force microscopy (AFM) scans with a resolution of 512 samples/line, an area of 5 × 5 μm^2, and a rate of 0.996 Hz. To roughly estimate the boron composition and to show the film's epitaxial nature, a x-ray diffraction (XRD) scan is performed using a Bruker D2 Phaser. To study the wurtzite and the zincblende phases in the film and to quantify the film quality, XRD scans were performed using a Bruker D8 Ultra. For the atomic-resolution scanning transmission electron microscopy measurement (STEM), an FEI Themis Z was operated at 200 kV with a probe size of 1–2 nm. The STEM lamella's thickness is around 50 nm. Rutherford backscattering spectrometry (RBS) and secondary ion mass spectrometry (SIMS) were performed to characterize the concentrations of different elements within the BGaN and AlN layers. RBS was combined with nuclear reaction analysis (NRA) to more accurately and directly estimate the boron composition in the BGaN film. He^{++} ions at an energy of 2.275 MeV with detector and grazing angles of 160° and 100°, respectively, were used for the RBS–NRA measurements. The SIMS conditions were tuned to give a depth resolution of around 8 nm in the BGaN layer. The H elemental background levels are tuned to ~10^{17} atoms/cm^3 in the BGaN film, while O and C are tuned to ~10^{15} atoms/cm^3.

Figure 2(a) shows an AFM scan on an area of 5 × 5 μm^2 of the BGaN surface. The root mean square (rms) roughness value is found to be 2.56 nm. Figure 2(b) shows the 2θ–ω scan of the sample, showing the BGaN, AlN, and sapphire peaks, and BGaN and AlN both

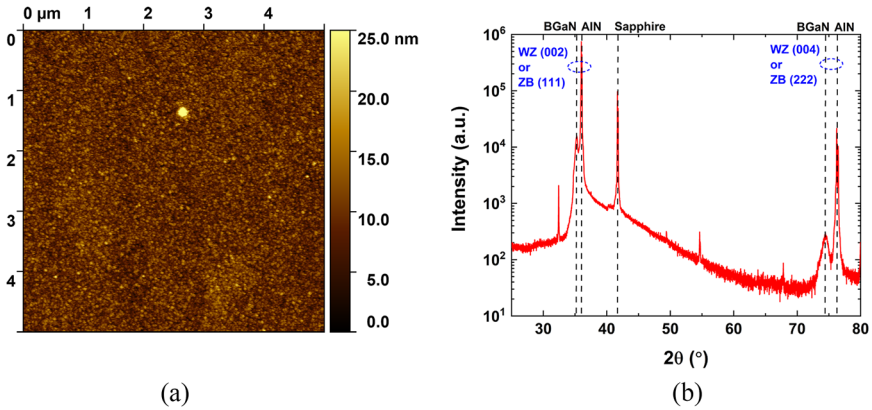

FIG. 2. (a) AFM scan of BGaN film with rms roughness value of 2.56 nm. (b) XRD 2θ–ω scan showing peaks from sample and template.

exhibit low and high order peaks, highlighting the epitaxial nature of the films. Using the 2θ peak, the boron composition of the BGaN film can be roughly estimated by linear interpolation between the GaN and BN peaks. Using this method, boron-to-III molar compositions of 10.2% and 9.7% are estimated, assuming wurtzite and zincblende films, respectively. By simply examining the 2θ–ω scan, it is difficult to determine whether a wurtzite phase or a zincblende phase occurs due to similarities in the inter-planar distances of the $(002)_{WZ}$ and the $(111)_{ZB}$ planes. This difficulty in discerning the phase necessitates better characterization approaches to distinguish the two phases.

Figure 3(a) depicts a pole figure scan that clearly shows reflections relating to the cubic and hexagonal phases. Unfortunately, the wurtzite BGaN peaks are too close to the AlN peaks, whereas the cubic peaks are too difficult to observe by 2θ–ω scans, thus making a precise phase-purity quantification difficult.[39] Additionally, high-resolution transmission electron microscopy (HRTEM) images and fast Fourier transform (FFT) of selected areas [Fig. 4(a)] confirm that the film is a wurtzite–zincblende mixture with stacking faults causing the mixed symmetry. Interestingly, the wurtzite and zincblende phases are quite similar on the atomic scale, where they can only be distinguished by observing the patterns in their layer stacking. The ABC stacking corresponds to the zincblende phase, whereas the ABAB stacking corresponds to the wurtzite phase [Figs. 3(b) and 3(c)].[40] The inset of Fig. 4(a) shows that the higher-order diffraction peaks, indicating the dominant phase, are missing. This trend is another characteristic of the mixed-phase material within the examined area.

The TEM image qualitatively shows the crystalline quality of our BGaN film on the atomic scale. To quantitatively estimate the average crystalline quality of the film, x-ray RC measurements were conducted [Fig. 4(b)]. The FWHM of the $(002)_{WZ}/(111)_{ZB}$ peak is only 810 arcsec. Although this is not at the same level as that of the highest-quality homo- and heteroepitaxial wurtzite III-nitride films, this crystalline quality is reasonably high for a high boron content BGaN alloy. Unfortunately, the majority of BGaN related works do not report the FWHM of XRD RCs. However, some of the reported values are by Kadys, Ougazzaden, and Gunning at 2500–9400, 2000–7000, and 250–3600 arcsec, respectively.[17,18,20]

Finally, RBS-NRA and SIMS were performed to characterize the concentrations of different elements within the BGaN and AlN layers. A boron-to-III molar composition of 15% ± 2% was determined using the RBS-NRA measurement [Fig. 5(a)]. The figure shows a small amount of gallium in the AlN regrowth layer, probably due to the MOCVD memory effect, where gallium sticks to the pipes and the flow channel then diffuses to the film during growth. Furthermore, Fig. 5(b) shows a considerable amount of boron in the AlN regrowth layer, which is likely due to a combination of the memory effect of boron and diffusion from the BGaN film, since boron is a small atom.

Interestingly, by using SIMS, a strong correlation is observed between the boron and hydrogen concentrations within the BGaN and AlN layers as the B-to-H ratio remains nearly constant at ~3:1. Unfortunately, SIMS cannot examine this correlation on the nanoscale. However, this result is somewhat reminiscent of the atom probe tomography measurement of BAlN.[41] Some insights are

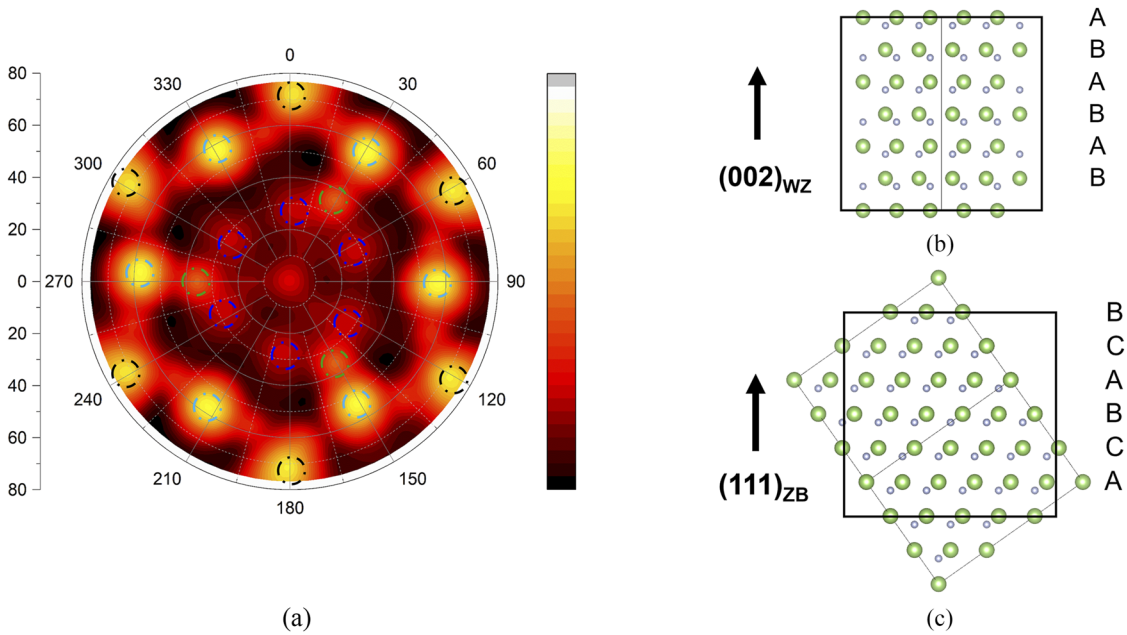

FIG. 3. (a) XRD pole figure at 2θ of 71.8°. The blue-dashed circles and the black circles are likely zincblende (311) and wurtzite (201) planes, respectively. The light-blue circles are likely a superposition of the zincblende (311) and the wurtzite (112). The green circles are the sapphire (208) planes. The zincblende peaks result from only BGaN, whereas the wurtzite peaks may be superposed AlN and BGaN peaks. (b) and (c) ABAB and ABC stacking of wurtzite and zincblende structures, respectively.

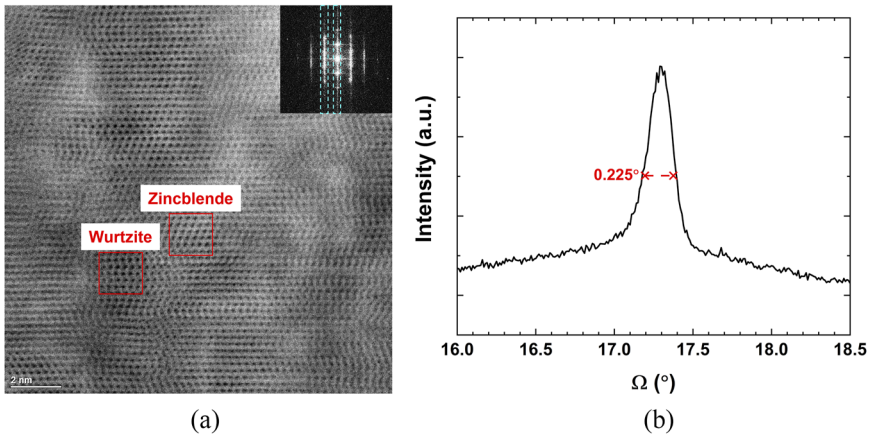

FIG. 4. (a) HRTEM image showing the mixed wurtzite and zincblende structures of the film. The inset FFT diffractogram highlights the lines corresponding to stacking faults indicating mixed hexagonal and cubic structures. The zone axis is (11-20) of the AlN template. (b) RC of the $(002)_{WZ}/(111)_{ZB}$ planes. The FWHM is 0.225° or 810 arcsec.

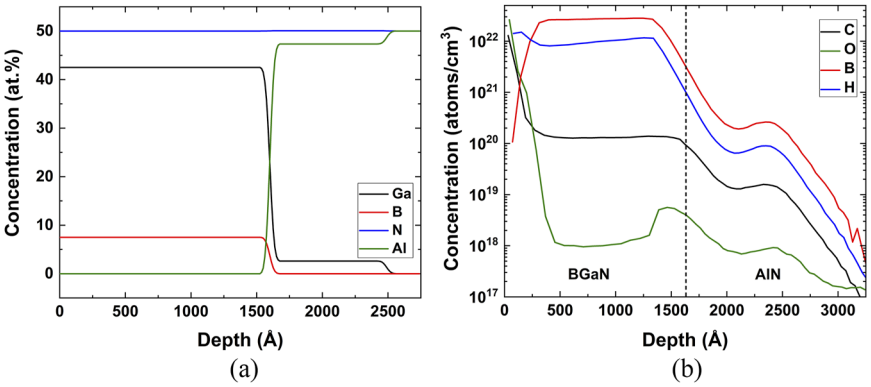

FIG. 5. (a) Simulated depth profile based on RBS-NRA measurement. Boron has an atomic concentration of 7.5 at. %, corresponding to a 15% III-nitride alloy composition. (b) SIMS measurement of B and various impurities in BGaN and AlN. B concentration using SIMS is not as precise as using RBS in the BGaN layer (top ~1600 Å).

provided by examining the theoretical calculations of the H impurities within BN, GaN, and AlN.[42,43] Based on these, we hypothesize that H is interstitial mostly between the B and N sites, acting as an amphoteric impurity. This hypothesis implies that H may prevent boron-containing nitrides from being conductive as H compensates the n- and p-type carriers in the film. As no H_2 is supplied during the BGaN growth, we believe this hydrogen comes from the decomposition of NH_3 and perhaps metalorganic sources. In addition, oxygen and carbon impurities were found in high quantities in the film, implying that the growth recipe needs further optimization to use BGaN as a functional material in electronic and optoelectronic devices.

In conclusion, a 200 nm thick, high-quality BGaN film was grown via MOCVD with a boron composition of 15%. The growth was performed at low temperature and pressure conditions of 600 °C and 75 Torr, respectively. TEB and TEG were used as source gases for boron and gallium, respectively. An rms roughness of 2.56 nm is determined via AFM scan on a $5 \times 5\ \mu m^2$ area. The XRD 2θ–ω scans implied a nearly lattice-matched BGaN/AlN film. A mixed-phase film was found via the XRD pole figure and HRTEM. Additionally, an 810 arcsec FWHM of the RC indicated a reasonably high crystalline quality of the $(002)_{WZ}/(111)_{ZB}$ planes. Moreover, a high boron composition of 15% was determined via RBS–NRA measurements. Finally, H, O, and C impurities were investigated using SIMS, and large quantities were detected in the BGaN film. We believe that the low growth temperature and the predicted band alignment might make it an ideal p-type layer in different device structures, such as LEDs and PIN neutron detectors.[21] However, further investigation is needed to reduce the impurities, which may affect its ability to conduct holes.

See the supplementary material for a discussion of why pure nitrogen, instead of the usual hydrogen, was used as a carrier gas in our growth.

The authors acknowledge the support of the KAUST Baseline Fund under Grant No. BAS/1/1664-01-01, Competitive Research under Grant Nos. URF/1/3437-01-01 and URF/1/3771-01-01, and the GCC Research Council under Grant No. REP/1/3189-01-01.

AUTHOR DECLARATIONS

Conflict of Interest

The authors have no conflicts to disclose.

Author Contributions

Feras AlQatari: Conceptualization (equal); Data curation (equal); Formal analysis (lead); Investigation (lead); Methodology (equal);

Writing – original draft (lead). **Che-Hao Liao**: Conceptualization (supporting); Data curation (equal); Formal analysis (supporting); Investigation (supporting); Methodology (equal); Writing – review & editing (equal). **Xiaohang Li**: Conceptualization (lead); Funding acquisition (lead); Project administration (lead); Writing – review & editing (equal).

DATA AVAILABILITY

The data that support the findings of this study are available within the article and its supplementary material.

REFERENCES

[1] O. Ambacher, J. Phys. D: Appl. Phys. **31**, 2653 (1998).
[2] J. H. Kim and P. H. Holloway, Appl. Phys. Lett. **84**, 711 (2004).
[3] M. J. Winiarski and D. A. Kowalska, Sci. Rep. **10**, 16414 (2020).
[4] L. M. R. Scolfaro, Phys. Status Solidi A **190**, 15 (2002).
[5] H.-M. Kim, Y.-H. Cho, H. Lee, S. I. Kim, S. R. Ryu, D. Y. Kim, T. W. Kang, and K. S. Chung, Nano Lett. **4**, 1059 (2004).
[6] O. Ambacher, J. Smart, J. R. Shealy, N. G. Weimann, K. Chu, M. Murphy, W. J. Schaff, L. F. Eastman, R. Dimitrov, L. Wittmer, M. Stutzmann, W. Rieger, and J. Hilsenbeck, J. Appl. Phys. **85**, 3222 (1999).
[7] M. Abid, T. Moudakir, G. Orsal, S. Gautier, A. En Naciri, Z. Djebbour, J.-H. Ryou, G. Patriarche, L. Largeau, H. J. Kim, Z. Lochner, K. Pantzas, D. Alamarguy, F. Jomard, R. D. Dupuis, J.-P. Salvestrini, P. L. Voss, and A. Ougazzaden, Appl. Phys. Lett. **100**, 051101 (2012).
[8] S. Watanabe, T. Takano, K. Jinen, J. Yamamoto, and H. Kawanishi, Phys. Status Solidi C **7**, 2691 (2003).
[9] M. Zhang and X. Li, Phys. Status Solidi B **254**, 1600749 (2017).
[10] A. Said, M. Debbichi, and M. Said, Optik **127**, 9212 (2016).
[11] K. Liu, H. Sun, F. AlQatari, W. Guo, X. Liu, J. Li, C. G. T. Castanedo, and X. Li, Appl. Phys. Lett. **111**, 222106 (2017).
[12] H. Sun, Y. J. Park, K.-H. Li, C. G. T. Castanedo, A. Alowayed, T. Detchprohm, R. D. Dupuis, and X. Li, Appl. Phys. Lett. **111**, 122106 (2017).
[13] X. Li, S. Wang, H. Liu, F. A. Ponce, T. Detchprohm, and R. D. Dupuis, Phys. Status Solidi B **254**, 1600699 (2017).
[14] M. E. Turiansky, J.-X. Shen, D. Wickramaratne, and C. G. Van de Walle, J. Appl. Phys. **126**, 095706 (2019).
[15] R. C. Cramer, J. English, B. Bonef, and J. S. Speck, J. Vac. Sci. Technol. A **37**, 061502 (2019).
[16] T. B. Tran, C.-H. Liao, F. AlQatari, and X. Li, Appl. Phys. Lett. **117**, 082102 (2020).
[17] B. P. Gunning, M. W. Moseley, D. D. Koleske, A. A. Allerman, and S. R. Lee, J. Cryst. Growth **464**, 190 (2017).
[18] A. Kadys, J. Mickevičius, T. Malinauskas, J. Jurkevičius, M. Kolenda, S. Stanionytė, D. Dobrovolskas, and G. Tamulaitis, J. Phys. D: Appl. Phys. **48**, 465307 (2015).
[19] F. AlQatari, M. Sajjad, R. Lin, K.-H. Li, U. Schwingenschlögl, and X. Li, Mater. Res. Express **8**, 086202 (2021).
[20] A. Ougazzaden, S. Gautier, T. Moudakir, Z. Djebbour, Z. Lochner, S. Choi, H. J. Kim, J.-H. Ryou, R. D. Dupuis, and A. A. Sirenko, Appl. Phys. Lett. **93**, 083118 (2008).
[21] A. Al Sulami, F. AlQatari, and X. Li, arXiv:2005.08407 (2020).
[22] A. Y. Polyakov, M. Shin, M. Skowronski, D. W. Greve, R. G. Wilson, A. V. Govorkov, and R. M. Desrosiers, J. Electron. Mater. **26**, 237 (1997).
[23] S. Gautier, G. Patriarche, T. Moudakir, M. Abid, G. Orsal, K. Pantzas, D. Troadec, A. Soltani, L. Largeau, O. Mauguin, and A. Ougazzaden, J. Cryst. Growth **315**, 288 (2011).
[24] T. Nakano, K. Mochizuki, T. Arikawa, H. Nakagawa, S. Usami, Y. Honda, H. Amano, A. Vogt, S. Schütt, M. Fiederle, K. Kojima, S. F. Chichibu, Y. Inoue, and T. Aoki, J. Appl. Phys. **130**, 124501 (2021).
[25] Y. Hasegawa, T. Akiyama, A.-M. Pradipto, K. Nakamura, and T. Ito, Phys. Status Solidi B **257**, 2000205 (2020).
[26] Q. Wang, R. Uddin, X. Du, J. Li, J. Lin, and H. Jiang, Appl. Phys. Express **12**, 011002 (2019).
[27] M. W. Moseley, D. D. Koleske, S. R. Lee, and A. A. Allerman, Report No. SAND2015-6354C, Sandia National Laboratory (SNL-NM), Albuquerque, NM, 2015.
[28] C. H. Wei, Z. Y. Xie, J. H. Edgar, K. C. Zeng, J. Y. Lin, H. X. Jiang, J. Chaudhuri, C. Ignatiev, and D. N. Braski, J. Electron. Mater. **29**, 452 (2000).
[29] A. Ougazzaden, S. Gautier, C. Sartel, N. Maloufi, J. Martin, and F. Jomard, J. Cryst. Growth **298**, 316 (2007).
[30] A. Ougazzaden, S. Gautier, T. Aggerstam, J. Martin, M. Bouchaour, T. Baghdadli, S. Ould Saad, S. Lourdudoss, N. Maloufi, Z. Djebbour, and F. Jomard, Proc. SPIE **6479**, 64791G (2007).
[31] T. Takano, M. Kurimoto, J. Yamamoto, M. Shibata, Y. Ishihara, M. Tsubamoto, T. Honda, and H. Kawanishi, Phys. Status Solidi A **180**, 231 (2000).
[32] K. Ueyama, H. Mimura, Y. Inoue, T. Aoki, and T. Nakano, Jpn. J. Appl. Phys. **55**, 05FD05 (2016).
[33] T. Akasaka and T. Makimoto, Jpn. J. Appl. Phys. **44**, L1506 (2005).
[34] T. Malinauskas, A. Kadys, S. Stanionytė, K. Badokas, J. Mickevičius, J. Jurkevičius, D. Dobrovolskas, and G. Tamulaitis, Phys. Status Solidi B **252**, 1138 (2015).
[35] K. Atsumi, Y. Inoue, H. Mimura, T. Aoki, and T. Nakano, APL Mater. **2**, 032106 (2014).
[36] E. B. Możdżyńska, S. Złotnik, P. Ciepielewski, J. Gaca, M. Wójcik, P. P. Michałowski, K. Rosiński, K. Piętak, M. Rudziński, E. Jezierska, and J. M. Baranowski, J. Mater. Sci. **57**, 7265 (2022).
[37] T. Honda, M. Kurimoto, M. Shibata, and H. Kawanishi, J. Lumin. **87-89**, 1274 (2000).
[38] D. A. Neumayer and J. G. Ekerdt, Chem. Mater. **8**, 9 (1996).
[39] M. Frentrup, L. Y. Lee, S.-L. Sahonta, M. J. Kappers, F. Massabuau, P. Gupta, R. A. Oliver, C. J. Humphreys, and D. J. Wallis, J. Phys. D: Appl. Phys. **50**, 433002 (2017).
[40] C. Stampfl and C. G. Van de Walle, Phys. Rev. B **57**, R15052 (1998).
[41] J. Sarker, T. B. Tran, F. AlQatari, C.-H. Liao, X. Li, and B. Mazumder, Appl. Phys. Lett. **117**, 232103 (2020).
[42] J. L. Lyons and C. G. Van de Walle, J. Phys.: Condens. Matter **28**, 06LT01 (2016).
[43] S. Limpijumnong and C. G. Van de Walle, Phys. Status Solidi B **228**, 303 (2001).